Large Eddy Simulation of transcritical and supercritical flows

Benedicte Cuenot, Schmitt Thomas

Large Eddy Simulation of transcritical and supercritical flows

B. Cuenot[1], T. Schmitt[2]

[1] *CERFACS, 42 A. G. Coriolis 31057 Toulouse,France*

[2] *Laboratoire EM2C, CNRS, CentraleSupélec, Université Paris-Saclay, 3 rue Joliot Curie, 91192 Gif-sur-Yvette cedex, France*

Abstract

Transcritical and supercritical flows are encountered in cryogenic rocket engines, where reactants are stored and injected at high pressure and low temperature. This implies specific thermodynamic and diffusive behaviors, which have direct impacts on the combustion and flow dynamics. To predict such systems, the Large Eddy Simulation approach is today commonly used as it allows a good description of the turbulence and other transient phenomena. The formulation involves the fully compressible flow equations, associated to a cubic equation of state and modified transport properties to properly describe the dense fluid. In the paper, the complete formulation is recalled and specific numerical treatments implemented in the code AVBP to ensure accuracy and robustness are described. Validation test cases as well as rocket engine applications are then presented to demonstrate the capacities of the numerical approach and the reliability of the models for such complex systems. Ongoing developments and future works are finally given.

1 Introduction

The combustion chamber in Liquid Rocket Engines (LRE) reaches extremely high pressure levels, exceeding the critical pressure (P_c) of most propellants. Depending on their injection temperature respectively to their critical one (T_c), reactants are injected in different thermodynamic conditions. With low P_c and T_c (12.8 bars and 33 K respectively), hydrogen, commonly used in LREs, is most of the time supercritical (i.e. gaseous) before burning. Liquid oxygen, having P_c = 50.5 bars is often injected at supercritical pressure and subcritical temperature (T_{c,O_2}=155 K), a regime generally referred to as transcritical. Today seen as a promising alternative fuel, methane has a P_c of 46.5 bars, i.e., much higher than hydrogen but still lower than usual chamber pressures, meaning also a supercritical regime. However in the context of LRE manufacturing and operating costs reduction, which introduces additional constraints linked to operational flexibility and engine reusability, methane may be either at subcritical or supercritical pressure and may even change state during a launch.

In the transcritical regime, the fluid thermodynamic behavior changes drastically and the ideal gas Equation of State (EoS) does not hold anymore [1]. Transport properties are also impacted and the surface tension vanishes. This supercritical fluid state has therefore direct consequences on the fuel injection, atomization and combustion processes occurring in the LRE. Instead of forming droplets as in subcritical conditions, the supercritical, dense fluid diffuses in the surrounding lighter fluid without forming a thin interface [2, 3]. This leads to modified mixing processes and, in turn, modified chemical activity. These phenomena have been observed in lab-scale experiments, for both LO_2/H_2 and LO_2/CH_4 [4, 5]. Measurements are however very difficult in such extreme conditions, and it is essential to have numerical tools for the understanding and prediction of flames, heat transfer and acoustics in LRE combustion chambers. If sufficiently reliable and accurate, such tools may be extremely useful for the design of LRE at a reduced cost in comparison with real tests.

2 Equations and models

Stable combustion in a LRE occurs in the turbulent, thin flame non-premixed regime. The very fast chemistry of H_2/O_2 leads to a flame anchored at the injector lips, i.e., a purely diffusion flame controlled by turbulent mixing [4]. As CH_4/O_2 chemistry is slower, the flame may detach and lead to a partially premixed combustion mode [5]. It is then important to include chemical kinetics in the model equations. Turbulence is treated with the Large-Eddy-Simulation (LES) approach for a good description of the intermittent flow structures and their interaction with the flame.

The governing equations therefore are based on the spatially filtered (in the sense of LES), fully compressible Navier-Stokes equations, added with species conservation equations and closed with a real-gas EoS. They write:

$$\frac{\partial \overline{\rho}\tilde{u_i}}{\partial t} + \frac{\partial}{\partial x_j}(\overline{\rho}\tilde{u_i}\tilde{u_j}) = -\frac{\partial}{\partial x_j}[\overline{P}\delta_{ij} - \overline{\tau_{ij}} + \tau^t_{ij}] \quad (1)$$

$$\frac{\partial \overline{\rho}\tilde{E}}{\partial t} + \frac{\partial}{\partial x_j}(\overline{\rho}\tilde{E} - \tilde{u_j}) = -\frac{\partial}{\partial x_j}[\tilde{u_i}(\overline{P}\delta_{ij} - \overline{\tau_{ij}}) + \overline{q_j} + q^t_j] + \overline{\dot{\omega}_T} \quad (2)$$

$$\frac{\partial \overline{\rho_k}}{\partial t} + \frac{\partial}{\partial x_j}(\overline{\rho_k}\tilde{u_j}) = -\frac{\partial}{\partial x_j}[\overline{J_{j,k}} + J^t_{j,k}] + \overline{\dot{\omega}_k} \quad (3)$$

where $\overline{\mathcal{Q}}$ and $\tilde{\mathcal{Q}}$ denote spatial and mass-weighted (Favre) spatial filter of any quantity $\mathcal{Q}$. In Eq. (1) to Eq. (3), which respectively correspond to the conservation laws for momentum, total energy and species, the following symbols (ρ, u_i, E, ρ_k) denote the density, the velocity components, the total energy per unit mass ($E = e_c + e$, with e the sensible energy) and the density of the chemical species k: $\rho_k = \rho Y_k$ for $k = 1$ to N (where N is the total number of species) with Y_k the mass fraction. P denotes the pressure, τ_{ij} the stress tensor, q_j the heat flux vector and $J_{j,k}$ the vector of the diffusive flux of species k. The source term in the species transport equations ($\dot{\omega}_k$ in Eq. (3)) comes from the consumption or production of species by chemical reactions. The source term in the total energy equation ($\dot{\omega}_T$ in Eq. (2)) is the heat release rate, which is the variation of sensible

enthalpy associated to species variation:

$$\dot{\omega}_T = -\sum_{k=1}^{N} \dot{\omega}_k h_k^0 \quad (4)$$

with h_k^0, the mass enthalpy of formation of species k. The stress tensor $\tilde{\tau_{ij}}$ is calculated from the filtered velocity, using a viscosity calculated with the Chung et al. method [6]. The species and heat fluxes (J_k and q) use classical gradient approaches, with a constant Schmidt (Sc_k) number while heat diffusion coefficient is also computed with the Chung et al. method. The subgrid scale quantities (stress tensor τ_{ij}^t, heat flux q^t, species flux J_k^t) are computed with a turbulent viscosity ν_t using the WALE model [7]. The above conservation equations are closed with a cubic EoS, either Peng-Robinson (PR) [8] or Soave-Redlich-Kwong (SRK) [9], which are very similar and can be written in the following generic form:

$$P = \frac{RT}{v-b} - \frac{\theta(T)}{v^2 + d_1 b v + d_2 b^2} \quad (5)$$

$$\text{PR} : (d_1, d_2) = (2, -1) \quad (6)$$

$$\text{SRK} : (d_1, d_2) = (1, 0) \quad (7)$$

where P is the pressure, T the temperature, v the molar volume ($v = W/\rho$ with W the mean molar mass of the mixture), $\theta(T)$ and b are parameters computed with respect to the critical points of the species contained in the mixture and their acentric factor.

Turbulent combustion modeling for diffusion flames is usually based on the flamelet concept. The flame structure is described as laminar strained flames, which are pre-tabulated in look-up tables as functions of the mixture fraction Z, for given boundary conditions and strain rates [10]. In the case of very fast chemistry as for H_2/O_2 combustion, the infinitely fast chemistry solution is a good approximation for the flame structure. In this case, only the equilibrium is tabulated with Z, and the source term $\dot{\omega}_k$ is calculated as a relaxation to equilibrium [11, 12]. The interaction with turbulence is then introduced using an β-function shape parameterized with the mixture fraction mean and variance. Flamelet approaches have demonstrated their capacity to accurately describe stable turbulent diffusion flames in rocket engines [12, 13, 14, 15]. However as they force a stable laminar flame structure, these methods are less performant in transient cases or in the occurrence of heat losses. These effects can be taken into account with the flamelet concept, but at the cost of extended look-up tables which may be difficult to build and costly to handle in CFD codes [16]. Other approaches may be used, with various levels of complexity and performance [17]. In particular, the direct integration of chemistry is very attractive as it is able to explicitly describe transient processes as well as the interaction of the flame with any flow feature [18] .

3 Applications

The above set of equations and models have been implemented in the code AVBP [19, 12], a third-order finite element solver on unstructured meshes [20]. Because of the non-linear nature of the thermodynamics, simulations of high-pressure flows are subject to stability issues [21]. The numerical stabilization method used in AVBP relies on artificial viscosity. Details are given in [22, 12]. For sufficiently refined meshes, the simulation naturally tends to Direct Numerical Simulation (DNS), which means the direct resolution of the full turbulence spectrum, i.e., without any model. As illustrated below this approach is useful to understand the details of physical processes.

In the following, the model is applied to various configurations of increasing complexity, to show the capacities of numerical study of transcritical and supercritical reacting flows.

3.1 DNS of flame stabilization behind a splitter plate

The mechanism of flame anchoring at the coaxial injector is critical as it ensures the flame stability. It is the result of the flow dynamics behind the splitter that separates the ergols, the combustion chemistry and the heat transfer in the splitter. To have a detailed description of these phenomena, DNS is performed in a simplified configuration, illustrated in Figure (1). In all cases below, chemistry is described with reduced chemical schemes accounting for about 10 species.

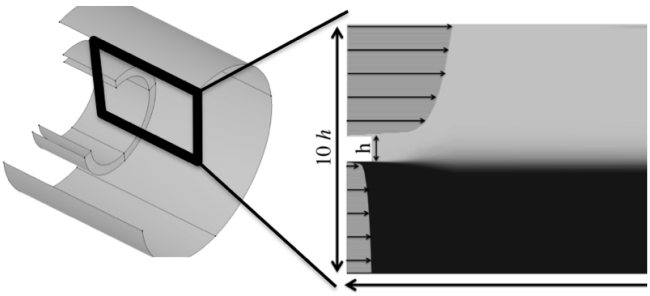

Figure 1: Configuration and 2D computational domain used in DNS of flame stabilization [23].

Ruiz et al. [23] performed the DNS of a H_2/O_2 transcritical flame at 10 MPa. In this benchmark case, light gaseous H_2 is injected at high speed and 150 K, while O_2 is transcritical at injection, at a temperature of 100 K and with a low velocity. The resulting density ratio is about 80, which is a very difficult challenge for numerics. The turbulence that develops behind the splitter requires typically a grid cell of $h/100$ where h is the splitter height. The obtained non-reacting flow is illustrated in Figure (2) (top) with an instantaneous snapshot of the density field. As expected for supercritical fluids, no atomization of the dense $O2$ is observed, replaced by the formation of elongated ligaments and diffusive mixing between the two ergols. After ignition a diffusion flame stabilizes at the splitter plate surface Figure (2) (bottom), where a small recirculation zone develops and allows the flame anchoring. The flame is highly wrinkled by the strong turbulence induced by the shear flow, but never quenches. The temperature increase in the burnt gas bring them back to perfect gas thermodynamics.

In [23] the splitter plate surface is considered adiabatic. The impact of heat losses on the flame anchoring mechanism was studied by Mari et al. [25], with coupled combustion - heat conduction simulations. Although the heat flux at the splitter tip reaches about 14 MW/m^2, the flame stays attached to the solid (Figure (3)). The heat loss is partially compensated by the pre-heating of the ergols along the splitter during injection, and by the near-wall chemistry, where the lower temperature favors the exothermic formation of radicals such as HO_2 and H_2O_2 as found for example in ignition. This explains the peak of heat release rate at the splitter tip, visible in

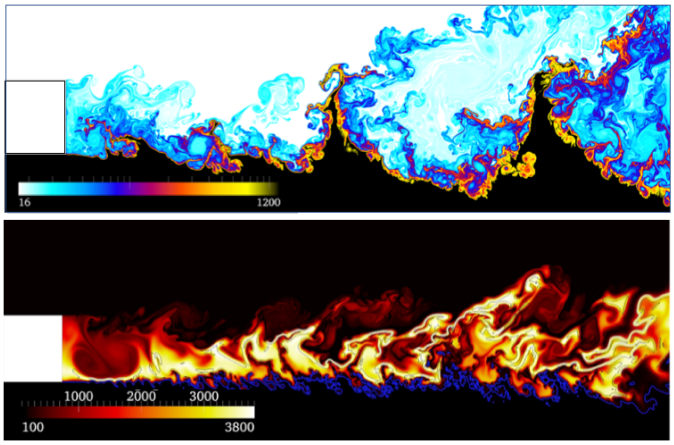

Figure 2: DNS of H_2/O_2 transcritical flow and flame: density [kg/m^3] in the non-reacting flow (top) and temperature [K] of the flame (bottom) [24].

Figure (3).

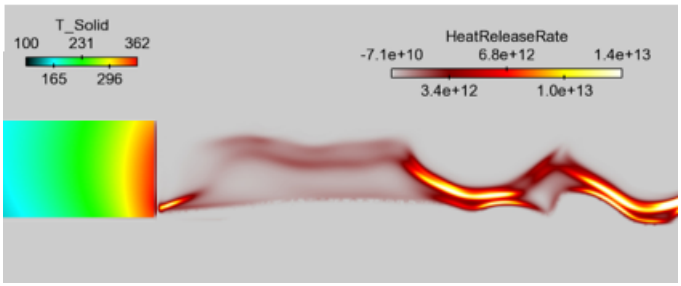

Figure 3: DNS of H_2/O_2 transcritical flame coupled with heat conduction in the splitter: heat release rate [J/m^3/s] and solid temperature [K] [25].

Recent DNS studies focused on CH_4/O_2 combustion, in doubly transcritical conditions [26]. Despite the 2D mesh and some uncertainty linked to chemical kinetics of high pressure methane oxy-combustion, the simulation revealed the underlying mechanisms of flame stabilization. Compared to H_2/O_2 flames, here the weaker flame leads to a more intermittent stabilization, allowing reactant leakage and partial premixing close to the wall. The impact of heat loss in coupled combustion - heat conduction simulations, in comparison with adiabatic surfaces, is found similar to the H_2/O_2 case described above, with a peak of heat release at the splitter tip (Figure (4)).

3.2 Validation : LES of a single injector configuration

The Mascotte test bench, operated at ONERA [3], has been specifically designed to study H_2/O_2 and CH_4/O_2 combustion in LRE conditions [3, 4]. It can reach chamber pressures up to 100 bars and has the capacity to apply transverse acoustic perturbations [27]. Although measurements are very difficult in these conditions, optical access and advanced laser techniques such as CARS or PLIF, as well as direct imaging give some information about the flame shape and stability. The configuration consists in a square combustion chamber of 50 mm side length, with lateral windows, fed with a coaxial injector and closed by a chocked nozzle.

For the purpose of validation, three test cases have been investigated in [12], named A60, C60 and G2 reproducing transcritical flames [28, 5]. Dense oxygen (i.e.

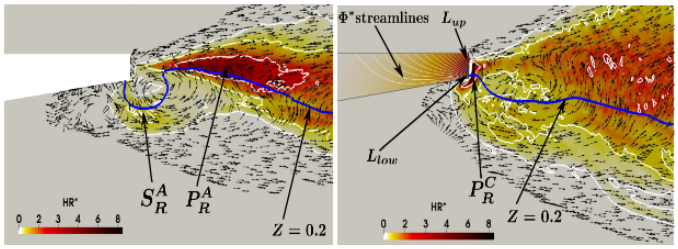

Figure 4: DNS of CH4/O2 doubly transcritical flame: adiabatic splitter plate (left) and coupled heat conduction in the splitter (right) [26]. Heat release rate (non-dimensionalized) and velocity vectors. The blue line is the isocontour of mixture fraction at 0.2, and Φ is the thermal flux. In the adiabatic case P_R^A and S_R^A are primary and secondary reaction zones, while only a primary zone P_R^C is observed in the coupled case. The flame intermittently anchors between locations L_{up} and L_{low}.

liquid-like oxygen) is injected at low velocity (less than 10 m/s), surrounded by gaseous hydrogen cases A60 and C60 or methane (case G2) flowing at high velocity (more than 100 m/s), in a chamber at supercritical pressure for both reactants (60 bar for case A60 and C60, 56 bar for case G2). Cases A60 and C60 only differ by the mass flow rate and injection velocity of H_2, 50 % larger for case A60 than C60.

The flow and flame structures are well illustrated with instantaneous views as shown in Figure (5) for case C60. A fully turbulent flame develops around the low velocity cold inner jet. High density oxygen pockets are produced downstream.

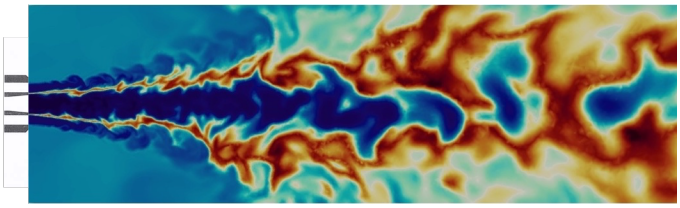

Figure 5: LES of MASCOTTE case C60. Longitudinal instantaneous field of temperature between 80 K and 3 600K [12].

A qualitative comparison with experiment is shown in Figure (6) for all three cases, where Abel transforms of OH* emission [28, 5] are compared with isocontours of the average OH mass fraction from the simulation (see [12] for OH* fields). Although the two quantities are not exactly equivalent, it can be seen that the topology of the flame is qualitatively recovered in all the cases, with a correct axial position of the opening and a proper flame length for cases A60 and G2. As in the experiment, the flame is found longer in case C60 compared with case A60, by near 100% in the LES, due to the smaller H_2 mass flow rate. In both cases the flame is attached to the injector lips, consistently with the DNS results of the above section. The absence of reactant leakage leads to purely diffusion flames, highly strained by the strong turbulence.

3.3 LES of a realistic rocket engine configuration

The numerical approach and modeling described above, and the computational power now available, allow today the simulation of multi-injectors, lab-scale engines. First

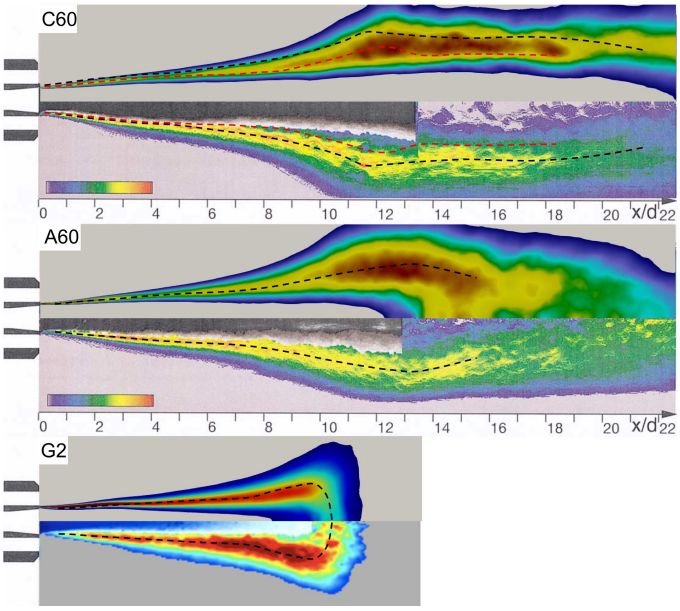

Figure 6: LES of MASCOTTE cases C60 (top), A60 (middle) and G2 (bottom). Comparison between the Abel transform of the average field of OH* emission [28, 5] and the average OH mass fraction from the simulation. Dashed lines show the top (in red) and bottom (in black) experimental flame position corresponding to the position of maximum emission [12].

steps were taken with simulations of combustion chambers with a limited number of injectors, in order to study possible interactions between flames and their impact on turbulent mixing, combustion efficiency and thermo-acoustic instabilities. With this objective, a five injectors combustor has been investigated experimentally at ONERA [27, 29]. The experimental facility allowed to apply transverse acoustic waves to the flames attached to the linearly arranged injectors. To gain better knowledge of the turbulent flames and their interaction, the experiment was computed using LES [29], for the operating conditions summarized in Table (1).

P_{ch} [MPa]	MR	J
6.7	1.1	3.7

Table 1: Chamber pressure, Mixture ratio MR, and momentum flux ratio J for the methane-oxygen five-injector case.

The simulations were able to reproduce both the non-modulated and the modulated cases, as illustrated in Figure (7), showing a good agreement with experiment. It can be seen that even in the non-modulated case, the flames interact as they widen under the effect of the developing turbulence. The transverse acoustic waves significantly reduce the flame length, and the dense core is notably shortened. This goes with an expansion in the transverse direction, leading to flattened flame shapes. The simulations allowed to analyze in detail the flow dynamics induced by transverse acoustics, as well as the flame response. In particular, the Rayleigh criterion showed a different behavior of the central and lateral flames, which produce larger heat release fluctuations. A complementary detailed study of the dynamics of a transcritical coaxial flame under a high-frequency transverse acoustic forcing is given in [30].

Today, LES of real rocket engine configurations with

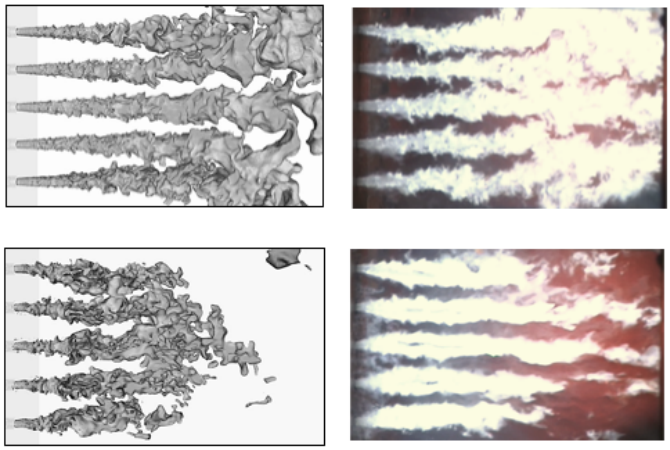

Figure 7: Instantaneous images of the five flames in the five-injector case [30]: numerical iso-surfaces of temperature (left) and experimental instantaneous light emission (right). Top: without modulation, bottom: with modulation.)

tens of injectors is feasible, although requiring important computational resources. Recently, the LES of a 42-injector rocket engine has been performed to study thermo-acoustic instabilities [31, 32]. The simulated BKD configuration operated at DLR Lampoldshausen [33] consists of a cylindrical combustion chamber of diameter 8 cm, closed by a choked nozzle (Figure (8)). The 42 coaxial injectors, arranged on the injection plate in three concentric rings, feed the combustor with hydrogen and oxygen in transcritical conditions. Both stable and unstable cases were observed experimentally. A stable case (LP1) and an unstable case (LP4) were simulated operating respectively at 70 bar and 80 bar. Note that in that case, a much coarser mesh than in previous single injector calculations was used. The impact of mesh resolution in single injector simulations was studied in [12], showing that the accuracy of stable flame prediction was kept on a coarse mesh similar to the one used for the BKD configuration. The impact of the mesh on combustion instability is however not yet fully assessed, and is the subject of current work.

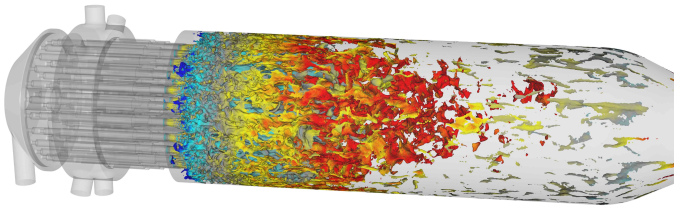

Figure 8: Overview of the BKD configuration: temperature isosurface colored with axial velocity [34].

In order to investigate the stability of the combustor, an external perturbation was applied in the LES in the form of a pressure perturbation corresponding to the first transverse mode of the chamber. In case LP1, the imposed perturbation is rapidly damped whatever its amplitude, confirming a stable operating point. On the contrary, case LP4 leads to a limit cycle for sufficiently high perturbation amplitudes, above 11 % of the chamber pressure. This means that for LP4 the LES is nonlinearly unstable. This is in agreement with the experimental observations, where case LP4 is unstable and case LP1 is stable. Pressure signals may be ana-

lyzed with spectral density plots as shown in Figure (9), also showing the experimental power spectral densities for comparison. Peak frequencies are observed at the same values in both LES and experiment, a first peak at 10700 Hz in the LES and 10260 Hz in the experiment, and a second peak at 21400 Hz in the LES and 20520 Hz in the experiment.

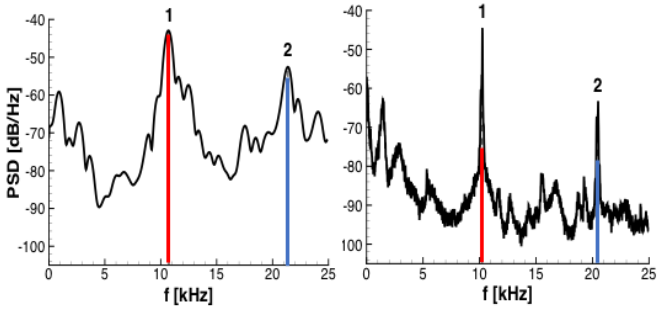

Figure 9: PSD of the pressure signal for LP4: comparison with experiment (raw experimental data courtesy of DLR, processed with the same tools as the LES results) [31, 32].

To characterize the stability of a combustor, the Rayleigh index R is used to measure the correlation between the flame power fluctuations q' and the pressure fluctuations p'.Positive R indicates a growing instability. The Rayleigh index obtained for both cases LP1 and LP4 and different pressure perturbation levels are reported in Table (2). First, R is always positive, meaning that pressure and combustion fluctuations always feed each other. As a consequence, stable cases can only be the result of energy losses through boundaries or dissipation. Second, R increases with the initial perturbation amplitude and reaches a maximum for LP4 with the largest perturbation. In this latter case, energy losses do not anymore counteract the fast instability growing and the combustor becomes unstable.

	LP1 [MPa]			LP4		
ΔP [bar]	2.5	5	8	2.5	5	10
R [kW]	32.5	39.9	65.9	23.9	29.1	143

Table 2: Rayleigh source term for different pressure amplitude ΔP [31, 32].

The objective of current studies is the prediction of the natural stability of the system and the transition between stable and unstable situations in order to identify the mechanisms leading to instability [34].

4 Conclusions

Although it remains challenging to compute transcritical and supercritical reacting flows, a numerical methodology is today available and validated. It allows to study complex phenomena such as ignition, combustion efficiency, flame stability or thermo-acoustic instabilities in real rocket engines. It can also be coupled to heat transfer simulation (conduction in solids and thermal radiation) to describe the combustion chamber thermal state and design efficient cooling systems [35]. The complexity of the physics involved, in particular the strong density gradients at injection, necessitate locally very fine meshes which induces extremely CPU cost: typically the simulation of the 42 injectors configuration required 100 000 CPU hours per ms of physical time on a BlueGene Q [31]. This demands a high parallel efficiency of the solver and the access to powerful computers.

Today a lot of efforts are devoted to the study of CH4/LOx thermo-kinetics effects on the engine behavior, in order to help the design of the new generation of rocket engines in the context of cost reduction and commercial competitiveness. In particular the modeling and simulation of the transition between supercritical and subcritical conditions has emerged as a key problem and is the subject of current research.

Acknowledgment

Support provided by ArianeGroup, the prime contractor of the Ariane launcher cryogenic propulsion system and CNES, the French National Space Agency, is gratefully acknowledged.

References

[1] J. C. Oefelein and V. Yang, "Modeling high-pressure mixing and conbustion processes in liquid rocket engines," *Journal of Propulsion and Power* , vol. 14, no. 5, pp. 843–857, 1998.

[2] M. Oschwald, J. J. Smith, R. Branam, J. Hussong, A. Shick, B. Chehroudi, and D. Talley, "Injection of fluids into supercritical environments," *Combustion Science and Technology*, vol. 178, pp. 49–100, 2006.

[3] M. Habiballah, M. Orain, F. Grisch, L. Vingert, and P. Gicquel, "Experimental studies of high-pressure cryogenic flames on the Mascotte facility," *Combustion Science and Technology*, vol. 178, no. 1, pp. 101–128, 2006.

[4] S. Candel, M. Juniper, G. Single, P. Scouflaire, and C. Rolon, "Structure and dynamics of cryogenic flames at supercritical pressure," *Combustion Science and Technology* , vol. 178, pp. 161–192, 2006.

[5] G. Singla, P. Scouflaire, C. Rolon, and S. Candel, "Transcritical oxygen/transcritical or supercritical methane combustion," *Proceedings of the Combustion Institute*, vol. 30, no. 2, pp. 2921–2928, 2005.

[6] L. L. Lee, K. E. Starling, T. H. Chung, and M. Ajlan, "Generalized multiparameters corresponding state correlation for polyatomic, polar fluid transport properties.," *Industrial and Chemical Engineering Research*, vol. 27, pp. 671–679, 1988.

[7] F. Nicoud and F. Ducros, "Subgrid-scale stress modelling based on the square of the velocity gradient," *Flow, Turbulence and Combustion* , vol. 62, no. 3, pp. 183–200, 1999.

[8] D. Peng and D. B. Robinson, "A new two-constant equation of state," *Ind. Eng. Chem. Fundam.*, vol. 15, pp. 59–64, 1976.

[9] G. Soave, "Equilibrium constants from a modified redlich-kwong equation of state," *Chemical Engineering Science* , vol. 27, pp. 1197–1203, 1977.

[10] N. Peters, "Laminar diffusion flamelet models in non-premixed turbulent combustion," *Progress in energy and combustion science*, vol. 10, pp. 319–339, 1984.

[11] T. Schmitt, Y. Méry, M. Boileau, and S. Candel, "Large-eddy simulation of oxygen/methane flames under transcritical conditions," *Proceedings of the Combustion Institute*, vol. 33, no. 1, pp. 1383–1390, 2011.

[12] T. Schmitt, "Large-eddy simulations of the mascotte test cases operating at supercritical pressure," *Flow, Turbulence and Combustion*, 2020.

[13] P. C. Ma, D. Banuti, J.-P. Hickey, and M. Ihme, "Numerical framework for transcritical real-fluid reacting flow simulations using the flamelet progress variable approach," in *55th AIAA Aerospace Sciences Meeting*, p. 0143, 2017.

[14] H. Huo and V. Yang, "Large-eddy simulation of supercritical combustion: Model validation against gaseous h 2–o 2 injector," *Journal of Propulsion and Power*, vol. 33, no. 5, pp. 1272–1284, 2017.

[15] J. Zips, H. Müller, and M. Pfitzner, "Efficient thermo-chemistry tabulation for non-premixed combustion at high-pressure conditions," *Flow, Turbulence and Combustion*, vol. 101, no. 3, pp. 821–850, 2018.

[16] B. Fiorina, R. Baron, O. Gicquel, D. Thevenin, S. Carpentier, and N. Darabiha, "Modelling non-adiabatic partially premixed flames using flame-prolongation of ildm," *Combustion Theory and Modelling*, vol. 7, pp. 449–470, 2003.

[17] M. Ma and C. Devaud, "A conditional moment closure (cmc) formulation including differential diffusion applied to a non-premixed hydrogen-air flame," *Combustion and Flame*, vol. 162, pp. 144–158, 2015.

[18] G. Lacaze, B. Cuenot, T. Poinsot, and M. Oschwald, "Large eddy simulation of laser ignition and compressible reacting flow in a rocket-like configuration," *Combustion and Flame*, vol. 156, pp. 1166–1180, 2009.

[19] V. Moureau, G. Lartigue, Y. Sommerer, C. Angelberger, O. Colin, and T. Poinsot, "High-order methods for DNS and LES of compressible multicomponent reacting flows on fixed and moving grids," *Journal of Computational Physics* , vol. 202, no. 2, pp. 710–736, 2005.

[20] O. Colin and M. Rudgyard, "Development of high-order taylor-galerkin schemes for unsteady calculations," *Journal of Computational Physics* , vol. 162, no. 2, pp. 338–371, 2000.

[21] G. Lacaze, T. Schmitt, A. Ruiz, and J. Oefelein, "Comparison of energy-, pressure-and enthalpy-based approaches for modeling supercritical flows," *Computers and Fluids*, vol. 181, pp. 35–56, march 2019.

[22] T. Schmitt, L. Selle, A. Ruiz, and B. Cuenot, "Large-Eddy Simulation of Supercritical-Pressure Round Jets," *AIAA Journal*, vol. 48, no. 9, 2010.

[23] A. Ruiz, B. Cuenot, L. Selle, and T. Poinsot, "The flame structure of a turbulent supercritical hydrogen/oxygen flow behind a splitter plate," in *47th AIAA/ASME/SAE/ASEE Joint Propulsion Conference & Exhibit*, p. 6121, 2011.

[24] A. Ruiz, *Unsteady Numerical Simulations of Transcritical Turbulent Combustion in Liquid Rocket Engines.* Phd thesis, Univ. Toulouse, 2012.

[25] R. Mari, B. Cuenot, J. Rocchi, L. Selle, and F. Duchaine, "Effect of pressure on hydrogen / oxygen coupled flame-wall interaction," *Combustion and Flame*, vol. 168, pp. 409–419, 2016.

[26] C. Laurent, L. Esclapez, D. Maestro, G. Staffelbach, B. Cuenot, L. Selle, T. Schmitt, F. Duchaine, and T. Poinsot, "Flame–wall interaction effects on the flame root stabilization mechanisms of a doubly-transcritical lo 2/lch 4 cryogenic flame," *Proceedings of the Combustion Institute*, vol. 37, no. 4, pp. 5147–5154, 2018.

[27] Y. Méry, L. Hakim, P. Scouflaire, L. Vingert, S. Ducruix, and S. Candel, "Experimental investigation of cryogenic flame dynamics under transverse acoustic modulations," *Compt. Rend. Mécan.*, vol. 341, pp. 100–109, 2013. Special issue "Combustion for Aerospace Propulsion".

[28] M. Juniper, A. Tripathi, P. Scouflaire, J. Rolon, and S. Candel, "Structure of cryogenic flames at elevated pressures," *Proceedings of the Combustion Institute*, vol. 28, no. 1, pp. 1103–1110, 2000.

[29] L. Hakim, A. Ruiz, T. Schmitt, M. Boileau, G. Staffelbach, S. Ducruix, B. Cuenot, and S. Candel, "Large eddy simulations of multiple transcritical coaxial flames submitted to a high-frequency transverse acoustic modulation," *Proceedings of the Combustion Institute*, vol. 35, no. 2, pp. 1461–1468, 2015.

[30] L. Hakim, T. Schmitt, S. Ducruix, and S. Candel, "Dynamics of a transcritical coaxial flame under a high-frequency transverse acoustic forcing: Influence of the modulation frequency on the flame response," *Combustion and Flame*, vol. 162, no. 10, pp. 3482–3502, 2015.

[31] A. Urbano, L. Selle, G. Staffelbach, B. Cuenot, T. Schmitt, S. Ducruix, and S. Candel, "Exploration of combustion instability triggering using large eddy simulation of a multiple injector liquid rocket engine," *Combustion and Flame*, vol. 169, pp. 129–140, 2016.

[32] A. Urbano, Q. Douasbin, L. Selle, G. Staffelbach, B. Cuenot, T. Schmitt, S.Ducruix, and S.Candel, "Study of flame response to transverse acoustic modes from the les of a 42-injector rocket engine," *Proceedings of the Combustion Institute*, vol. 36, no. 2, pp. 2633–2639, 2017.

[33] S. Gröning, D. Suslov, J. S. Hardi, and M. Oschwald, "Influence of hydrogen temperature on the stability of a rocket engine combustor operated with hydrogen and oxygen," *CEAS Space Journal*, pp. 1–18, 2016.

[34] T. Schmitt, G. Staffelbach, S. Ducruix, S. Gröning, J. Hardi, and M. Oschwald, "Large-eddy simulations of a sub-scale liquid rocket combustor: influence of fuel injection temperature on thermo-acoustic stability," in *7TH European Conference for Aeronautics and Aerospace Sciences (EUCASS)*, 2017.

[35] D. Maestro, B. Cuenot, and L. Selle, “Large eddy simulation of combustion and heat transfer in a single element gch 4/gox rocket combustor,” *Flow, Turbulence and Combustion*, vol. 103, pp. 699–730, 2019.